

## FEATURE ARTICLE

## Surface Plasmons on Metal Nanoparticles: The Influence of Shape and Physical Environment

Cecilia Noguez\*

*Instituto de Física, Universidad Nacional Autónoma de México, Apartado Postal 20-364, México D.F. 01000, México**Received: October 4, 2006; In Final Form: December 23, 2006*

The surface plasmon response of metal nanoparticles is studied for different shapes and physical environments. For polyhedral nanoparticles, the surface plasmon resonances are studied as a function of the number of faces and vertices. The modification of these surface plasmons by different surrounding media and the presence of a substrate or other nanoparticles is also discussed. We found that polyhedral nanoparticles composed with less faces show more surface plasmon resonances, and as the nanoparticle becomes more symmetric, the main surface plasmon resonance is blue-shifted. It is also found that the corners induce more surface plasmons in a wider energy range. In the presence of a substrate, multipolar plasmon resonances are induced, and as the nanoparticle approaches the substrate, such resonances are red-shifted. The interaction among nanoparticles also induces multipolar resonances, but they can be red or blue-shifted depending on the polarization of the external field.

## I. Introduction

Recent advances that allow metals to be structured and characterized on the nanometer scale have renewed the interest of physicists, chemists, materials scientists, and biologists in surface plasmons. Surface plasmons are collective excitations of the electrons at the interface between a conductor and an insulator and are described by evanescent electromagnetic waves that are not necessarily located at the interface. Surface plasmons appear in a number of different phenomena, including the optical response of materials at different scales, to Casimir and van der Waals forces between macroscopic bodies.<sup>1,2</sup> The strong coupling between light and surface plasmons in nanostructures leads to novel phenomena such as optical force enhancement in nanoaggregates,<sup>3</sup> transport and storage of energy,<sup>4</sup> as well as its localization and guiding,<sup>5–7</sup> surface-enhanced sensing and spectroscopy,<sup>8</sup> controlling the anisotropic growth of nanoparticles,<sup>9,10</sup> and measuring intramolecular and conformational distances in molecules.<sup>11</sup> The understanding of surface plasmon resonances (SPRs) provides a design rule that guides the development of more complex nanostructures with an optimal optical response that we can both predict and experimentally realize.<sup>12,13</sup>

The optical response of metal nanoparticles (NPs) can be tuned by controlling their size, shape, and environment, providing a starting point for emerging research fields like surface plasmon-based photonics or plasmonics.<sup>4</sup> On the other hand, new synthesis methods developed to fabricate nanoparticles (NPs) with a specific size and shape enable us to tailor SP properties for clearly defined applications.<sup>14</sup> For instance, SPs are now being investigated for their potential applications in

optics, magneto-optic, photonics, as a nanoengineered substrate on which the surface-enhanced Raman scattering response can be precisely controlled and optimized, and for chemical and biosensing applications, such as optical addressable diagnostic methods, devices, and therapies based on the plasmonic response of NPs.<sup>15</sup>

A clear and general interpretation of SPR in metal NPs is not available today. For instance, the one to one correspondence between the SP resonances and the morphology of realistic NPs is still awaiting. In recent years, the influence of the geometry on the optical properties of metal nanoparticles has been an active research field. Several studies have shown that the main optical features depend on geometry and size, and the optical response of spherical, spheroidal, cubic,<sup>16–18</sup> and other geometrical shapes, like rods<sup>19,20</sup> and triangular prisms,<sup>9</sup> are now well identified. However, it is known that metal nanoparticles of few nanometers show different structural motifs, such as icosahedra, octahedra, cuboctahedra, decahedra, etc.,<sup>21–27</sup> depending on their size, composition, and energetic conditions.<sup>28–30</sup> Furthermore, NPs can present both crystalline and noncrystalline arrangements and sometimes showing chiral structures.<sup>31–36</sup>

Additionally to the technological implications, the optical signature of the NPs is also used as a characterization tool. The latter is interesting because optical techniques are nondestructive, and with proper implementation, they can be used to perform measurements in situ and in real time, providing statistical properties of the whole sample. These attributes of optical spectroscopies are important because the properties of nanoparticles depend on the environment,<sup>16,18</sup> and when growth and characterization are made in different conditions, the environment might be an additional uncontrollable variable for the optical interpretation. Thus, optical spectroscopies can be used also as complementary tools of structural characterization

\* To whom correspondence should be addressed. E-mail: cecilia@fisica.unam.mx.



**Cecilia Noguez** was born in Mexico City, Mexico in 1966. She pursued a B.S. degree in Physics from the National University of Mexico (UNAM) in 1990, working in effective medium theories for the optical response of nanocomposites. In 1993, she received a M.S. degree and in 1995 a Ph.D. degree both in physics at UNAM working with Prof. Ruben G. Barrera. During her doctorate studies, she spent one year at the University of Rome “Tor Vergata” in Italy, studying the optical response of semiconductor surfaces working with Prof. Rodolfo Del Sole. In 1995, she was a postdoctoral research assistant at the Department of Physics & Astronomy at Ohio University, working on silicon clusters with Profs. Sergio E. Ulloa and David A. Drabold. In 1996, she joined the Solid State Department at the Instituto de Fisica at UNAM, where she was promoted to Associated Professor in 2003 and to Full Professor in 2005. Her current research focuses on the physics of metal nanoparticles, chiral nanostructures, semiconductor surfaces, and van der Waals forces in real materials.

techniques like atomic force microscopy (AFM), scanning tunneling microscopy (STM), transmission electron microscopy (TEM), etc.,<sup>21–27</sup> which provide the image of a small piece of the sample, giving information about local properties and characterizing few NPs at a time.

In this article, we give some insights of the SPRs as function of the morphology for NPs of different shapes. We also discuss how these SPRs are modified by changing the physical environment. In particular, we discuss the presence of a substrate or other nearby NPs. In the case of silver, many results indicate the presence of icosahedra and decahedral shapes as well as other related morphologies like cubes and truncated cubes.<sup>27</sup> These particles follow a very similar pattern to other metallic NPs.<sup>29</sup> Here, we show that the proper SPRs of metal NPs and their intensity are determined uniquely by their morphology and size. We establish specific trends of the SPRs in terms of the faces, vertices, and other geometrical parameters. Based on this, we show that, once the optical signature of a NP with a specific geometry and made of an arbitrary material is known, it would be possible to predict the behavior of the SPRs if the material and ambient are changed. For this, we will introduce the concept of spectral representation<sup>37–39</sup> that we will use to predict the optical response of elongated NPs of different aspect ratio immersed in various ambient.

This article is organized as follows. In section II, we introduce the principles of the light interaction with NPs. The ingredients to find the optical response of NPs of arbitrary shapes and sizes are discussed. In section III, we present the concept of surface plasmon resonances, and we briefly introduce the spectral representation formalism that allows us to study the optical response as a function of the NPs’ geometry. In section IV, we apply the spectral representation formalism to elongated NPs, showing the potential of this technique. In section V, we discuss the influence of the morphology in the SPRs, showing how they

are tailored with the NP shape. In section VI, the influence of the physical environment on the optical response is studied. First, we show how the presence of a substrate modifies the SPRs, and then, we discuss how the positional disorder of one-dimensional (1D) arrays of NPs influences the optical response. Finally, a summary and future trends are presented in section VII.

## II. Light Interaction with Small Particles

When a particle is under the action of an electromagnetic (EM) field, its electrons start to oscillate, transforming energy from the incident EM wave into, for example, thermal energy in an absorption process. The electrons can also be accelerated, and then, they can radiate energy in a scattering process. In a typical experimental setup the attenuation by the sum of scattering and absorption of an electromagnetic wave going through a material is called the EM extinction. In this work, we consider a medium composed of NPs dispersed in a homogeneous medium, in such way that the interactions between particles are negligible.<sup>40</sup> Thus, the extinction,  $\sigma_{\text{ext}}$ , can be modeled as the optical response of one immersed NP times the particles concentration<sup>41</sup>

$$\sigma_{\text{ext}} = \mathcal{N}(C_{\text{abs}} + C_{\text{sca}}) \quad (1)$$

where  $\mathcal{N}$  is the number of particles per unit volume and  $C_{\text{abs}}$  and  $C_{\text{sca}}$  are the absorption and scattering cross sections of a single particle.

In this work, we consider NPs, which are large enough to employ classical EM theory. However, they are still enough small to observe the dependence of the optical properties with their size and shape. This means that the inhomogeneities of the particle are much smaller compared to the wavelength of the incident EM field, such that, each point of the NP can be described in terms of a macroscopic dielectric function, which depends on the frequency and sometimes on its size, as we explain in section II.A. Here, we restrict ourselves to the elastic or coherent case, where the frequency of the absorbed and scattered light is the same as the frequency of the incident light. There is an unfortunate tendency to assume that bulk dielectric functions are inapplicable to small particles with intense shape-dependence absorption. We emphasize, however, that these effects can usually be explained satisfactorily with classical EM theory and the size-adapted bulk dielectric constants.

The optical response of a NP characterized by a dielectric function  $\epsilon(\omega)$  is obtained by solving the Maxwell equations in matter. In 1908, Gustav Mie found the exact solution to the Maxwell equations for the optical response of a sphere of arbitrary size immersed in a homogeneous medium, subjected to a plane monochromatic wave.<sup>42,43</sup> On the other hand, rigorous solutions of the Maxwell equations for nonspherical particles are not straight forward. Only few exact solutions are known: the case of spheroids by Asano and Yamamoto<sup>44</sup> and for infinite cylinders by Lind and Greenberg.<sup>45</sup> Thus, the optical properties of NPs with other arbitrary shapes can be found only in an approximate way.<sup>46</sup> For example, the Gans approximation can be applied to ellipsoids with very transparent material, where the refractive index is very small and the size is small compared with wavelength.<sup>47,48</sup> Because of the complexity of the systems being studied, efficient computational methods capable of treating large size materials are essential. In the past few years, several numerical methods have been developed to determine the optical properties of nonspherical particles, such as the discrete dipole approximation (DDA), the T-matrix, spectral

representation, finite differences methods, etc.<sup>46</sup> Once a numerical method is chosen, it is important to select a “realistic” dielectric function that better resembles the material properties of the system, in this case, particles of nanometric sizes. Here, we show the main characteristics that a realistic dielectric function should have to calculate the light extinction of NPs.

**A. Nanoparticle Dielectric Function.** As starting point, we can employ dielectric functions measured experimentally for bulk metals,  $\epsilon_{\text{exp}}(\omega)$ . These dielectric functions have contributions from interband (inter) and intraband (intra) electron transitions, which we can assume are additive

$$\epsilon_{\text{exp}}(\omega) = \epsilon_{\text{inter}}(\omega) + \epsilon_{\text{intra}}(\omega) \quad (2)$$

Interband contributions are due to electron transitions from occupied to empty bulk bands separated by an energy gap. The electrons are bound by a restoring force given by the energy difference between ground and excited electronic states in metals, usually at the ultra violet (UV) region.<sup>41</sup> Intraband contributions come from electron transitions at the Fermi level in incompletely filled bands, or when a filled band overlaps in energy with an empty band. These transitions also provide an absorption mechanism but at lower energies. Electrons at the Fermi level in metals are excited by photons of very small energies, such that, they are essentially “free” electrons. The contributions from free electrons to  $\epsilon_{\text{exp}}(\omega)$  can be described by the Drude model<sup>41</sup>

$$\epsilon_{\text{intra}}(\omega) = 1 - \frac{\omega_p^2}{\omega(\omega + i/\tau)} \quad (3)$$

where  $\omega_p$  is the plasma frequency and  $1/\tau$  the damping constant due to the dispersion of the electrons. For most metals at room temperature,  $1/\tau$  is much less than  $\omega_p$ , and the plasma frequency for metals is usually in the visible and UV regions, with energies  $\hbar\omega_p$  from 3 to 20 eV. The theoretical values of  $\omega_p$  can disagree from those obtained experimentally, since the contribution from the bound electrons or interband transitions is not considered in the Drude model. In fact, the bound electrons create a positive background that screens the free electrons and  $\omega_p$  is usually pulled down. For instance, the Drude model predicts for silver a plasma frequency to be 9.2 eV,<sup>41</sup> but the measured one is actually 3.9 eV.<sup>49</sup>

The collision time  $\tau$  determines a characteristic distance  $\lambda_\tau$ , which plays a fundamental role in the theory of electron conduction. An electron picked at random at a given moment will, on average, travel a distance  $\lambda_\tau$  before its next collision. This distance  $\lambda_\tau$  is also known as the mean free path of electrons, and at room temperatures is of the order of few nanometers. Here, we are interested in small NPs mostly at room temperature; hence, we have to consider that electrons can be also dispersed by the NP surface, because the free electron’s mean free path is now comparable or larger than the dimension of the particle. Therefore, it is necessary to include an extra damping term  $\tau(a)$  to  $\epsilon_{\text{exp}}(\omega)$ , due to the surface scattering of the “free” electrons. The surface dispersion not only depends on the particle size, but also on its shape.<sup>50</sup>

To include surface dispersion we need modify the intraband contributions by changing the damping term. From eq 2, we obtain the input of the bound charges by subtracting the free electron contribution from the bulk dielectric function. The free electron contributions are calculated with Drude and using the theoretical values of  $\omega_p$ . Now, we include the surface damping by adding the extra damping term  $\tau(a)$  to the Drude model. Finally, we obtain a dielectric function, which also depends on

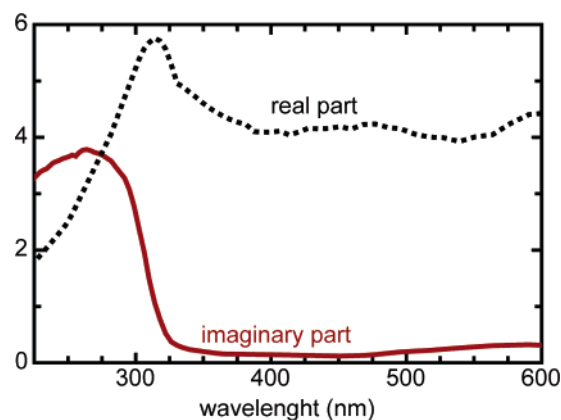


**Figure 1.** Interband contributions to the dielectric function of bulk silver.

the NP size, and includes the contributions of (i) the free electrons, (ii) surface damping, and (iii) interband transitions or bound electrons, given by

$$\begin{aligned} \epsilon(\omega, a) &= \epsilon_{\text{inter}}(\omega) + \epsilon_{\text{intra}}^{\text{NP}}(\omega, a) \\ &= \{\epsilon_{\text{exp}}(\omega) - \epsilon_{\text{intra}}(\omega)\} + \\ &\quad \left\{ 1 - \frac{\omega_p^2}{\omega(\omega + i/\tau + i/\tau(a))} \right\} \quad (4) \end{aligned}$$

In this work, we will consider for all the cases the surface dispersion of a sphere of radius  $a$  given by  $1/\tau(a) = v_f/a$ ,<sup>51</sup> where  $v_f$  is the Fermi velocity of the electron cloud. The smaller the particle, the more important is the surface dispersion effect. Later we will show that surface dispersion effects do not change the location of the surface modes, but they affect the coupling of such proper modes with the applied field, making the resonance peaks wider and less intense.<sup>18</sup>

In Figure 1, we show the interband or bound electrons input to the bulk dielectric function of silver as measured by Johnson and Christy,<sup>49</sup> according to eq 2, and using Drude to model the intraband input. The main contribution to the imaginary part of  $\epsilon_{\text{inter}}(\omega)$  is at wavelengths below 325 nm, whereas for larger wavelengths, the input is almost nil. On the other hand, the contributions to the real part are always different from zero, being the most significant at about 315 nm, while between 350 and 700 nm the real part is almost constant. We should keep in mind that interband electron transitions will absorb energy, but not contribute to SPRs.

Once the NP’s dielectric function is determined, we have to choose a method to find the SPRs. In this work, we employ the spectral representation formalism and the discrete dipole approximation (DDA). In section III, we introduce the main concepts of the spectral representation formalism, and in sections IV and VI, we employ it to study the SPRs of ellipsoidal NPs, as well as supported NPs and 1D chains. For the case of suspended polyhedral NPs, we employ DDA, which is a well suited technique for studying scattering and absorption of electromagnetic radiation by particles of arbitrary shapes with sizes of the order or less than the wavelength of the incident light.<sup>52</sup> For a more complete description of DDA and its numerical implementation, DDSCAT, the reader can consult refs 17 and 53–56.

**B. Large Nanoparticles versus Small Nanoparticles.** The importance of the absorption and scattering process as a function of the particle size can be studied for spherical particles using the Mie theory, see for example ref 18. It was found that for

NPs of less than 40 nm of diameter the radiation processes are negligible, and the particle only absorbs energy. On the other hand, the scattering effects dominate the response of NPs of 100 nm and larger.

1. *Small Particles (<40 nm)*. When the size of a homogeneous particle is much smaller than the wavelength of the incident light, the NPs feel a field spatially constant, but with a time dependent phase, which is known as the quasistatic limit. Small NPs absorb energy through the following mechanisms: (i) Collective excitations of the “free” electrons, which give rise to surface modes or surface plasmon resonances that are determined by the particle shape and variations of the dielectric function. (ii) Electron transitions of bound electrons from occupied to empty bulk bands of different index, also called interband transitions. (iii) Surface dispersion or scattering of the “free” electrons, when their mean free path is comparable to the dimension of the NP.

In the case of a small sphere, the displacement of the charges is done homogeneously, yielding a dipolar charge distribution on the surface. These charges give rise to only one proper resonance, which is determined uniquely by the shape of the NP and its electron density. This resonance is independent of the direction of the incident light, such that, only one proper mode is found, which is independent of the NP size. However, the proper resonances depend extremely on the NP’s shape. For example, ellipsoids with three different axes have tensor polarizabilities with three different dipole modes. Furthermore, as the particle becomes less symmetric, the induced charge distribution on the surface can result not only on dipolar modes with different resonant frequencies, but also on higher multipolar charge distributions, even in the quasistatic limit. For instance, the induced electronic cloud on cubic NPs is not distributed homogeneously on the surface, such that, extra multipolar charge distributions are clearly induced.<sup>17,18,37</sup> The high multipolar SPRs are always located at smaller wavelengths with respect to the dipolar one, which, additionally, is always red-shifted by the presence of the electric field generated by the higher multipolar charge distributions.

2. *Large Particles (>40 nm)*. When the size of the particle increases, the radiation effects become more and more important. The displacement of the electronic cloud is no longer homogeneous even for spherical particles, and once more, high multipolar charge distributions are induced. This fact can be seen from the Mie theory, where the extinction and scattering cross sections are expressed in series expansion of the involved fields, which are described in terms of spherical harmonic functions, such that, the different multipolar excitations and their contribution can be easily identified.<sup>43</sup> For instance, in a recent experiment, up to hexa-multipolar charge distributions have been observed in large spherical NPs.<sup>57</sup> Furthermore, the accelerated electrons produce an additional polarization field that depends on the ratio between the size of the particle and the wavelength of the incident light.<sup>58</sup> Because of this secondary radiation, the electrons lose energy experiencing a damping effect, which makes wider the SPRs.<sup>18</sup> This field reacts against the quasistatic polarization field and shifts the position of the modes to larger wavelengths. Thus, the radiation damping reduces the intensity and makes broader and asymmetric the SPR peaks, which are red-shifted.

In summary, the optical signature of small particles is given by the SPRs that depend on the NPs shape, which are associated to different surface charge distributions that are explained in terms of different multipolar moments. The SPRs are influenced by the NP size, such that, for particles of few nanometers the

resonances do not change their position or frequency, but they become wider because of surface dispersion effects. When the size increases the SPRs are now affected by the secondary radiation, which moves their position to smaller frequencies and makes broader the peaks. Besides, light scattering is also present, which induces the excitation of new SPRs of higher multipolar order.

In conclusion, to describe the optical response of NPs, it is crucial to understand the number, position, and width of the SPRs as a function of the NP shape, size, and environment.

### III. Surface Plasmons: General Theory

When conduction electrons oscillate coherently, they displace a electron cloud from the nuclei giving rise to a surface charge distribution. The Coulomb attraction between positive and negative charges results in restoring forces, characterized by oscillation frequencies of the electron cloud with respect to the positive background, which are different from those of the incident EM wave. Each collective oscillation with different surface charge distribution is known as surface plasmon resonance (SPR). The number of such modes as well as their frequency and width are determined by the electron density, effective mass, particle’s shape, size, dielectric function, and its environment. In this work, we are interested in the surface plasmon response of metal NPs; therefore, we consider particles whose sizes are much smaller than the wavelength of the incident light, where the quasi-static limit is still valid.

**A. Surface Plasmons.** Let us consider a NP composed of a homogeneous, isotropic, and nonmagnetic material with dielectric function  $\epsilon(\omega)$ . The NP is embedded in a nonmagnetic host with dielectric constant  $\epsilon_h$ . Under the action of an incident EM wave, the free charges are displaced producing a polarization field  $\vec{P}$ . The light absorption is given by the proper modes of the NP, which are specified by  $\vec{P}$ . The proper modes responsible for the optical absorption satisfy  $\nabla \cdot \vec{P} = \nabla \times \vec{P} = 0$ , inside the particle, but  $\nabla \cdot \vec{P} \neq 0$ , on the surface. These surface modes are evanescent electromagnetic waves, which are not necessarily localized near the surface, but they are accompanied by a polarization charge  $\nabla \cdot \vec{P}$  on it. We should recall that bound electrons do not participate in the collective motion of the electron cloud, thus, SPRs are quite independent of the interband contributions to the dielectric function, except that they can act as a positive background changing in some way the environment of the free electrons.

In the existing theories, the frequencies of the resonant proper modes and their coupling strength to the applied field cannot be immediately calculated, because they involve a procedure that usually requires taking the nondissipation limit, which calls for a vast amount of numerical effort. However, we can construct a theory that yields both the frequencies of the proper modes and the size of their coupling strength to the applied field by building a spectral representation of the effective polarizability of the system. In this representation, the effective polarizability is expressed as a sum of terms with single poles, such that, the location of the poles is associated with the frequencies of the normal modes through a spectral variable, and their strength with the coupling of these modes to the applied field. The spectral representation has advantages over other theories, because it separates the contribution of the dielectric properties from the geometrical ones. The latter allows us to perform a systematic study of the optical response of NPs: once a shape is chosen, the frequencies of the plasmon resonance of particles of different size and dielectric properties can be calculated with a minimum numerical effort. Next we present a brief introduction to the spectral representation formalism.

**B. Spectral Representation Formalism.** The spectral representation formalism was first introduced by Fuchs to study the optical properties of ionic crystal cubes.<sup>37</sup> In this seminal paper, Fuchs showed that the particle's polarizability can be written as a sum over normal modes. Later, Bergman<sup>38</sup> and Milton<sup>39</sup> showed that the effective local dielectric function of any two-phase composite in 3D can always be written in terms of a spectral representation. The main advantage of this representation is that the proper modes do not depend on the dielectric properties of the components but only on the geometry of the system. Moreover, from the explicit expressions of the spectral representation, we can easily obtain the strength of the coupling of different optically active modes with the applied field, whose frequency is determined by the poles of the polarizability.

Within the spectral representation, the NP's polarizability  $\alpha(\omega)$  is expressed as a sum of terms with single poles<sup>37</sup>

$$\frac{4\pi}{v}\alpha(\omega) = -\sum_n \frac{C(n)}{s(\omega) - s_n} \quad (5)$$

where  $C(n)$  is the spectral function, which gives the strength of each eigenvalue  $s_n$ , and  $v$  is the NP volume. The spectral variable  $s(\omega)$  is defined in terms of the dielectric properties of the components as<sup>37</sup>

$$s(\omega) = \frac{1}{1 - \epsilon(\omega)/\epsilon_h} \quad (6)$$

The  $n$ th SPR given by the  $n$ th pole of eq 5 has a complex frequency  $\Omega_n = \omega_n + i\gamma_n$ , which satisfies  $s(\Omega_n) = s_n$ , where the real frequency,  $\omega_n$ , gives the location of the proper mode, and  $\gamma_n$  gives its relaxation rate. Furthermore, it has been shown<sup>38</sup> that the eigenvalues are real numbers between  $0 \leq s_n \leq 1$ , and the spectral function satisfies the sum rule<sup>37</sup>

$$\sum_n C(n) = 1$$

which means that the total strength of all modes is conserved. Now, substituting the dielectric function from eq 4 into the spectral variable expression in eq 6, the frequency  $\Omega_n$  of the  $n$ th eigenmode is given by

$$\Omega_n = \omega_n + i\gamma_n = -i\Gamma + \sqrt{-\Gamma^2 + \omega_p^2 s_n A_n} \quad (7)$$

with  $A_n = [s_n(\epsilon_{\text{inter}} + 1 - \epsilon_h) + \epsilon_h]^{-1}$  and  $2\Gamma = 1/\tau + 1/\tau(a)$ .

From here, we can infer some general behavior of the SPRs. For instance, if the relaxation time decreases ( $\Gamma$  increases), the frequency of the SPR is always red-shifted. However, this shift is very small since for typical metals  $\Gamma \ll \omega_p$ . Now, when the particle is immersed in vacuum  $\epsilon_h = 1$ , and assuming that there are not contributions from interband transitions ( $\epsilon_{\text{inter}} = 0$ ), we obtain that  $A_n = 1$ , such that,  $\omega_n = \omega_p \sqrt{s_n}$ . For a homogeneous sphere, it has been found that there is a single mode with  $s_n = 1/3$  and  $C(n) = 1$ , such that, by substituting in eq 5, one obtains the well-known expression of the sphere polarizability.

Otherwise  $A_n < 1$ , such that, the SPRs are always red-shifted with respect to vacuum. Furthermore, we find that the shift is not just by a constant because it depends on the proper mode itself: the smaller the eigenvalue  $s_n$  is, the larger the red shift is. Therefore, we found that the location of the surface plasmon resonances is sensitive to the dielectric environment, and as the refraction index increases, the spectrum suffers a red shift and becomes wider. This is because the red-shift is larger for

resonances at greater wavelength. However, the number of resonances is still the same independently of the refraction index of the host medium.

The main advantage of the spectral representation is that the location of the poles and their strength are independent of the size and dielectric properties of the particle and depend only on its shape. To show the capabilities of the spectral representation formalism, we will study in detail the case of elliptical particles, where an explicit expression of the spectral representation of the polarizability is easily found. This case is useful to illustrate how the eigenvalues  $s_n$  depend on the geometrical parameters, and how the frequencies of these proper modes can be easily obtained. Although the proper modes and their strength are independent of the NPs size and dielectric properties, explicit values of these are difficult to obtain. Until now, the spectral representations of different NPs have been found only for spherical, ellipsoidal, and cubic geometries, as well as for colloidal suspensions of spherical particles, and supported ellipsoidal NPs, which we will employ in section VI.

#### IV. Elongated Nanoparticles

Metal nanoellipsoids possess three plasmon resonances corresponding to the oscillation of electrons along the three axes of the NP. The resonance wavelength depends on the orientation of the electric field relative to the particle. By changing the axes length, the plasmon resonance frequencies of the nanoellipsoid can be tuned systematically. The possibility of tuning the optical response of NPs has attracted the attention of scientists, and a large variety of new synthesis methods have been developed to fabricate elongated NPs.<sup>59–71</sup> When these NPs are dispersed in a matrix (solid or liquid), the random orientation leads to an average absorption spectrum containing the three plasmon resonances. On the other hand, when the axes of the nanoellipsoids are oriented in the same direction, it is possible to distinguish between the different resonances by using polarized light.<sup>70,71</sup>

In this section, we employ the spectral representation to obtain the SPR of nanoellipsoids as a function of their geometrical parameters and independent of the dielectric properties. This allows us to do a systematic study of the SPRs of gold and silver elongated NPs with different aspect ratios and immersed in different media. Finally, we study the case of aligned spheroids and the dependence of the SPRs on light polarization. The reader can consult recent reviews by Murphy et al.<sup>72</sup> and Pérez-Juste et al.,<sup>73</sup> which provide a nice overview of the synthesis and properties of elongated NPs.

##### A. Spectral Representation of Ellipsoidal Nanoparticles.

Let us consider an ellipsoidal NP under the action of a uniform external electric field. The ellipsoid has a volume  $v_e = (4\pi/3)abc$ , where  $a$ ,  $b$ , and  $c$  are its semi-axes. The components of the ellipsoid's dipolar polarizability is<sup>74</sup>

$$\alpha_\gamma(\omega) = \frac{v_e}{4\pi} \frac{\epsilon(\omega) - \epsilon_h}{\epsilon_h + L_\gamma[\epsilon(\omega) - \epsilon_h]} \quad (8)$$

where  $\gamma$  denotes  $x$ ,  $y$ , or  $z$  and  $L_\gamma$  are functions of  $a$ ,  $b$ ,  $c$ , and the eccentricity  $e$ . Notice that  $L_\gamma$  are independent of the material properties of the ellipsoid and depend only on the geometrical parameters. Using the definition of the spectral variable in eq 6, we can rewrite each component  $\gamma$  of the ellipsoid's polarizability, as

$$\frac{4\pi}{v_e}\alpha_\gamma(\omega) = -\frac{1}{s(\omega) - L_\gamma} \quad (9)$$

**TABLE 1: Eigenvalues of the SPRs of Prolates and Oblates Spheroids of Different Aspect Ratios**

$a:c$ $s_n$	1:2 $L_x, L_z$	1:4 $L_x, L_z$	1:6 $L_x, L_z$	1:8 $L_x, L_z$	1:10 $L_x, L_z$	1:20 $L_x, L_z$
prolate	0.1735, 0.4132	0.0754, 0.4623	0.0432, 0.4784	0.0284, 0.4858	0.0203, 0.4898	0.0067, 0.4966
oblate	0.2363, 0.5272	0.1482, 0.7036	0.1077, 0.7846	0.0845, 0.8308	0.0695, 0.8608	0.0369, 0.9262

In this case, we can easily identify the geometrical factors with the eigenvalues of the surface proper modes of the spheroid,  $s_n = L_\gamma$ , and their strength are  $C_\gamma = 1/3$ . Thus, the eigenvalues are independent of the material properties of the ellipsoid, and the SPRs are given by the poles of eq 9. Taking into account the definition of the spectral variable, we find that these SPRs fulfill the condition  $\epsilon(\omega)L_\gamma + \epsilon_h(1 - L_\gamma) = 0$ . Now, it is necessary to calculate the depolarization factors  $L_\gamma$ .

For simplicity, let us consider ellipsoids generated by the rotation of an ellipse around its major or minor axes, which produce prolate or oblate spheroids, correspondingly. Since prolate and oblate NPs have a symmetry axis, they have three proper modes, where two of them are degenerated. The geometrical factors  $L_\gamma$  for prolate spheroids ( $a > b = c$ ) are<sup>74</sup>

$$L_x = \frac{1 - e^2}{2e^3} \left( \log \frac{1 + e}{1 - e} - 2e \right)$$

$$L_y = L_z = 1/2(1 - L_x) \text{ and } e = \sqrt{1 - b^2/a^2} \quad (10)$$

Whereas for oblate spheroids ( $a = b > c$ ), they are

$$L_z = \frac{1 + e^2}{e^3} (e - \tan^{-1} e)$$

$$L_x = L_y = 1/2(1 - L_z) \text{ and } e = \sqrt{a^2/c^2 - 1} \quad (11)$$

For a sphere ( $a = b = c$ ), it is evident that the depolarization factors are all degenerated, and to satisfy the sum rule condition, they must be equal to  $L_x = L_y = L_z = 1/3$ , and the SPR fulfills the well-known expression  $\epsilon(\omega)L_\gamma + \epsilon_h(1 - L_\gamma) = \epsilon(\omega) + 2\epsilon_h = 0$ .

In the previous section, we found a general behavior of the SPRs, where a red shift of the modes is found when the particle is immersed in a host media, and when interband electrons transitions are present. To make a closer analysis of the SPRs of elongated NPs and without loss of generality, let us assume that the NP is immersed in vacuum and its dielectric function does not contain contributions from interband transitions, and  $\Gamma \ll \omega_p$ , such that  $\omega_n = \omega_p \sqrt{s_n}$ . In this case, the frequency of the resonance for the sphere is given by the well-known expression  $\omega_{n=1} = \omega_p \sqrt{3}$ . Now, let us analyze the case for prolate particles when the semi-axis  $a$  goes to  $\infty$ , and a cylinder or needle with its axis along  $x$  is obtained. Then, the depolarization factors are  $L_x \rightarrow 0$ ,  $L_y = L_z \rightarrow 1/2$ , such that, as  $a$  increases, the mode along the symmetry axis is red-shifted until it ceases to be visible (zero frequency), while the two perpendicular modes converge to  $\omega_n = \omega_p \sqrt{2}$ . The other limit case is for oblates when  $a$  and  $b \rightarrow \infty$  that corresponds to a flat plate or disk, and the depolarization factors  $L_x = L_y \rightarrow 0$  and  $L_z \rightarrow 1$ . Here, the two identical modes along the symmetry axis cease, since their resonances go to zero as  $a$  and  $b \rightarrow \infty$  while the perpendicular one  $\omega_n \rightarrow \omega_p$ . In Table 1, we show the depolarization factors for prolate and oblates spheroids as a function of the aspect ratio  $a:c$ . We observe that for an aspect ratio  $a:c = 6:1$  (1:6) for prolates (oblates), the limit cases mentioned previously have been already attained within a 10%.

**B. Application to Gold and Silver NPs.** To exhibit the potentiality of the spectral representation, here, we perform a systematic study of the SPRs of ellipsoidal gold and silver NPs that are immersed in different media. In the following, we define the aspect ratio of the NP as the length of the major axis divided by the width of the minor axis. We will also label the modes as longitudinal (LM) when they are along the symmetry axis of the particle, whereas transversal modes (TM) are those excited in the perpendicular direction. Let us consider gold (Au), and silver (Ag) NPs with theoretical  $\hbar\omega_p = 8.55$  and 9.2 eV, respectively. The NPs are embedded in a medium with refraction index  $n = \sqrt{\epsilon_h}$ . For visible wavelengths, the contributions of interband transitions can be approximated by a constant,  $\epsilon_{\text{inter}} \approx 9.9$  for Au and  $\epsilon_{\text{inter}} \approx 3.9$  for Ag. With these parameters, we calculate the dielectric function according to eq 4, and using the eigenvalues  $n_s$  from Table 1, and substituting in eq 7, the frequency of the LM and TM modes of prolate and oblates NPs can be obtained with minimum numerical effort.

In Figure 2, we plot the position of the resonance as a function of the aspect ratio for gold prolate (left side) and silver oblate (right side) NPs, embedded in vacuum with  $n = 1$ , water/glycerol with  $n = 1.3$ , dimethyl sulfoxide or silica glass with  $n = 1.47$ , sapphire with  $n = 1.77$  or TiO<sub>2</sub> with  $n = 2.79$ . In general, we confirm that, as the refraction index of the host media increases, all of the modes are always red-shifted. The LM of prolate particles behaves as the TM of oblate NPs, where the position of the modes is displaced to larger wavelengths as the aspect ratio increases, although the shift is smaller for oblates than for prolates. In the same way, the TM of prolates behaves similarly to that of the LM of oblates, but now, the modes are shifted to smaller wavelengths when the aspect ratio increases, and this shift is larger for oblates than for prolates. We observe that the LMs and TMs of prolates and oblates, respectively, show a linear behavior independently of the refraction index  $n$ , where the slope is modified by  $n$  as well as by the particular shape. For instance, the slope of the LMs of prolates is larger than that of the TMs of oblates. On the other hand, the TM (LM) of prolates (oblates) shows a behavior inversely proportional to the aspect ratio. The TMs of prolates are always blue-shifted, and for aspect ratios between 1 and 3, it occurs rapidly, whereas from 4.5 and larger the limit value is almost reached. Furthermore, the limit value of LMs of oblates is slightly shifted to large wavelengths as  $n$  increases, whereas for prolates the limit value of TMs is more susceptible to the value of  $n$ .

The linear behavior of the modes of elongated NPs has been observed experimentally and theoretically in nanorods and nanodisks.<sup>59–67</sup> In some of these works, phenomenological equations to determine the position of the resonances have been proposed. However, these empirical models can be applied only to a specific system, where the slope of the linear equation depends on the solution where the particles are dispersed. On the other hand, using the expressions for the eigenvalues given in eqs 10 and 11, we find an exact dependence of the SPR position as a function of the aspect ratio. For instance, let us consider the case when the spheroid is nearly spherical ( $e \ll 1$ ), such that, the longitudinal eigenvalues of prolates and oblates NPs are approximately<sup>74</sup>

$$s_{\text{LM}}^{\text{prolate}} = \frac{1}{3} - \frac{2}{15}e^2, \text{ and } s_{\text{TM}}^{\text{oblate}} = \frac{1}{3} + \frac{2}{15}e^2$$

respectively. Since  $e^2$  is inversely proportional to the aspect ratio for prolates, and proportional for oblates, we find from eq 7 that the frequencies of LMs for prolates are inversely proportional to the aspect ratio, whereas they are proportional to it for oblates. Also from eq 7, we find that all modes are inversely proportional to  $\epsilon_h$ . Now, considering that the wavelength is inversely proportional to the frequency,  $\lambda = c/\omega$ , we obtain that the position of the LMs of prolates is proportional to the aspect ratio, while for oblates is inversely proportional. Additionally, the modes are proportional to the refraction index  $n$  in all cases. These explain the behavior of the resonances in Figure 2, as well as the observations of experimental and theoretical works.<sup>59–67</sup> Notice that deviations from a prolate ellipsoidal shape have effects on the optical properties of nanorods.<sup>64,67</sup>

**C. Aligned Elongated Nanoparticles.** To show the sensitivity of anisotropic NPs to polarized light, we simulate the optical absorbance of prolate spheroids with a small aspect ratio of 1.6 and a major axis of 8 nm, which are embedded in silica ( $n = 1.47$ ). The optical absorbance of the nanocomposites has been calculated by controlling the angle  $\theta$  of the wavevector  $\mathbf{k}$  of the incident electromagnetic field with respect to the major axis of the NP. The polarization of the incident electric field was varied at different angles  $\phi$  with respect to the minor axis and perpendicular to  $\mathbf{k}$ . In Figure 3, panels a and b, the simulated absorbance spectra are shown for the incident electromagnetic field at  $\theta = -45^\circ$  and  $90^\circ$ , respectively, and different angles of polarization. When  $\theta = -45^\circ$  in Figure 3a, it is observed that for  $\phi = 0^\circ$  the electric field is along the minor axis exciting only the surface plasmon at 375 nm. Conversely, when the angle of polarization is  $\phi = 72^\circ$ , both resonances are excited, but the one at 375 nm is weaker than the resonance at 470 nm. Similarly, when  $\theta = 90^\circ$  in Figure 3b, the wavevector  $\mathbf{k}$  is almost aligned to one of the minor axes, and as a consequence, the electric field is polarized along the other minor axis at  $\phi = 0^\circ$  and almost along the major axis at  $\phi = 72^\circ$ . Finally, if we consider that  $\theta = 0^\circ$  (not shown in the figure), the wavevector  $\mathbf{k}$  is along the major axis, in such a way that the electric field mostly excites the resonance at 375 nm for any polarization. Similar conclusions have been found recently for metal nanorods.<sup>71</sup>

Recently, the shape and alignment of metallic NPs embedded in insulator matrices have been controlled using MeV ion beam irradiation.<sup>69,70</sup> Symmetric NPs were transformed into anisotropic particles whose larger axis is along the ion beam. Upon irradiation, the surface plasmon resonance of symmetric particles split into two resonances whose separation depends on the fluence of the ion irradiation.<sup>70</sup> Simulations of the optical absorbance showed that the anisotropy is caused by the deformation and alignment of the nanoparticles and that both properties can be controlled with the irradiation fluence.<sup>70</sup>

## V. Shape Influence on the Surface Plasmons

In the case of metal NPs, many results indicate the presence of polyhedral shapes with well-defined facets and vertices, like icosahedral (IH) and decahedral (DH) NPs, as well as fcc related morphologies like cubes and truncated cubes (TC).<sup>28,29,57,75–79</sup> To understand the influence of morphology, the SPRs for polyhedral NPs have been recently studied.<sup>80</sup> A general relationship between the SPRs and the morphology of each NP was established in terms of their vertices and faces. The optical response was investigated for cubes and DHs, as well as for different truncations of them.<sup>80</sup> Here, we show results for cubic and DH silver NPs whose volume is equal to that of a sphere with a radius of 2.2 nm, which are immersed in a media with a refraction index  $n = 1.47$ . The extinction efficiencies,  $Q_{\text{ext}}$ , were calculated using DDA with the order of  $10^5$  polarizable entities, which ensure the convergence of the optical response for each NP. We employ the measured bulk dielectric function for silver by Johnson and Christy,<sup>49</sup> which is modified according to eq 4 to incorporate the surface dispersion effects.

**A. Cubic Morphology.** We first study  $Q_{\text{ext}}$  for a nanocube, and then, we compare it to those obtained for different TCs, the IH, and the sphere. In Figure 4, we show  $Q_{\text{ext}}$  for a silver nanocube immersed in a medium with  $n = 1.47$  (solid line) and in vacuum (dashed line). In both spectra, we observe that the optical response below 325 nm follows the same behavior independently of the dielectric properties of the surrounding media, since at those wavelengths and smaller the main absorption mechanism is due to the interband transitions. Therefore, this structure should also be independent of the morphology of the NP, as we will show later when we compare  $Q_{\text{ext}}$  for different TCs. At larger wavelengths, both spectra show

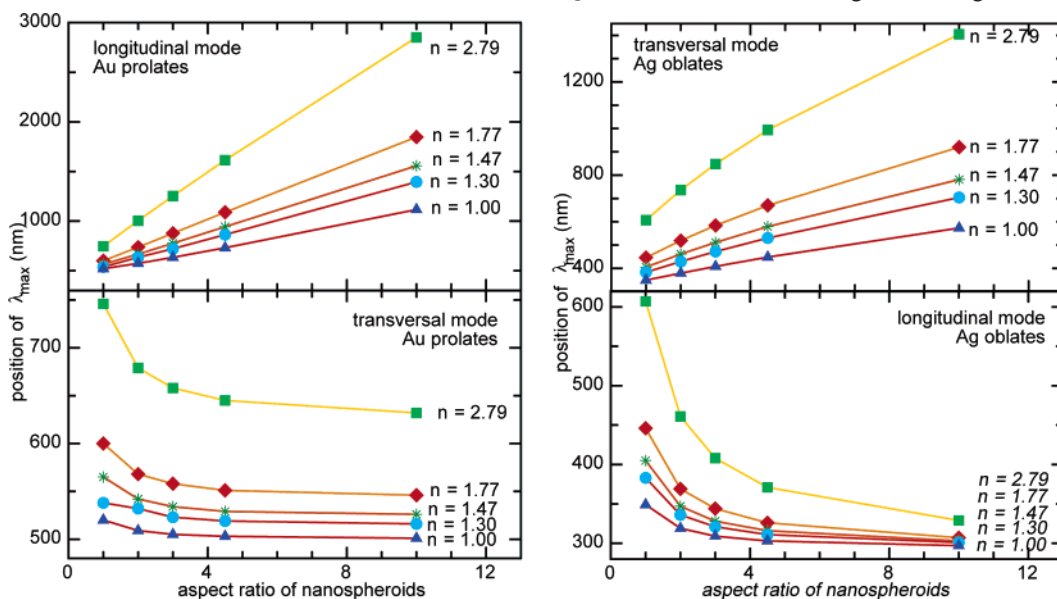


**Figure 2.** Positions of LM and TM surface plasmon resonances of gold prolate (left side) and silver oblate (right side) NPs with different aspect ratios and embedded in various media. The lines are just for guidance.

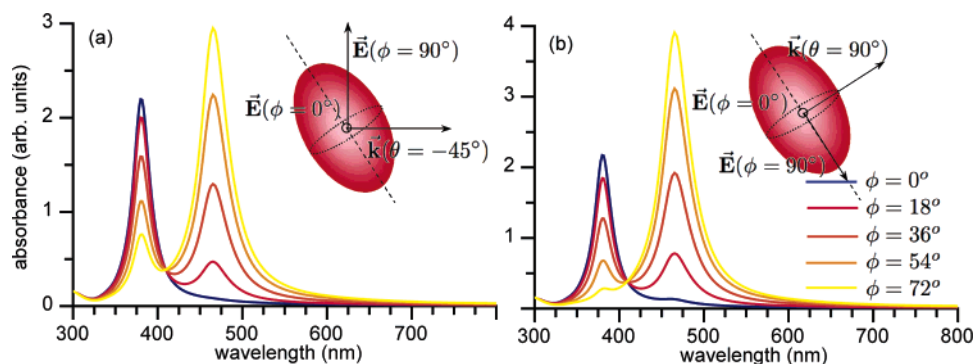


**Figure 3.** Simulated optical absorbance for linear-polarized light from  $0^\circ$  to  $90^\circ$ . The polarization indicated in the second plot is the same for all. The wavevector of the incident electromagnetic field respect to the major axis is depicted.

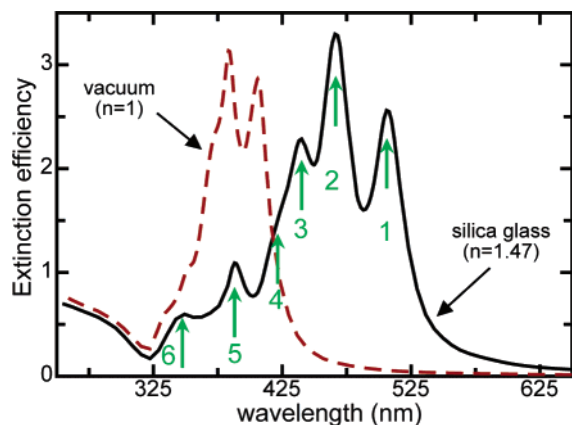


**Figure 4.** Extinction efficiency of a silver cube nanoparticle as a function of the wavelength of the incident light, and immersed in vacuum and in silica. The main six surface plasmon resonances are indicated.

a rich structure of peaks, which is better observed when  $n = 1.47$ . We mentioned in section III that, for media with  $n > 1$ , the spectrum is red-shifted with respect to vacuum. Furthermore, this shift is not just by a constant, because it depends on the proper mode itself. It is clear from Figure 4 that the SPRs are spread out as  $n > 1$ , and the red shift is larger for SPRs at greater wavelengths. For instance, when  $n = 1.47$ , we can identify six SPRs more easily than when  $n = 1$ . These six resonances were found by Fuchs,<sup>37</sup> who calculated nine SPRs where only six of them account for more than the 96% of the spectrum. The SPRs 1 and 2 correspond to the dipolar and quadrupolar charge distributions and are located at 506 and 466 nm, respectively, and their amplitude is particularly high at the corners. The modes 3–6 are at smaller wavelengths and show higher multipolar charge distributions. The amplitude of modes 5 and 6 is high at the center of the faces, whose normal points along the electric field.<sup>37</sup>

Now, let us compare  $Q_{\text{ext}}$  of a nanocube to those for different TCs, the IH and the sphere. The TCs are obtained by truncating the eight corners of the cube by  $l \times r$ , where  $l$  is the length of the cube's side and  $0 < r \leq 1/2$ . We label the different truncations with the number  $r$ . When  $r = 1/2$  a cuboctahedron (CO) is obtained. Six octagons and eight triangles compose all of the TCs, except the CO that is composed by six planar squares and eight triangles. All of the TCs have 14 faces. Finally, if we performed a symmetric truncation of the cube with a larger number of planes, one could arrive to the IH, and with an infinite number of planes to the sphere. In Figure 5, the extinction efficiencies of TCs with  $r$  from  $1/8$  to  $1/2$  are shown. The optical response below 325 nm is the same independently of the morphology, as expected. It is observed that, even for the

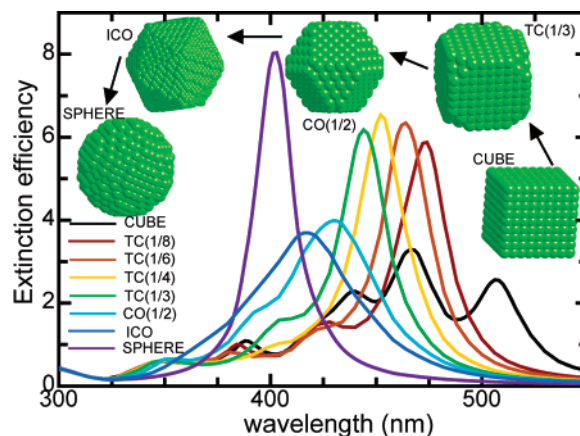


**Figure 5.** Extinction efficiencies as a function of the wavelength of the incident light of a silver cube, different truncated cubes, and a spherical nanoparticle.

smallest truncation ( $r = 1/8$ ), the SPRs are very sensitive to the morphology. In this case, the dipolar SPR is blue-shifted about 30 nm. The location of the dipolar and quadrupolar SPRs are now very close, such that, only one wide peak is observed around 474 nm, which is more intense. The SPR 3 has vanished, and the others show a slightly blue shift. The same trend is observed for larger truncations, and when the CO is obtained with  $r = 1/2$ , the spectrum becomes wider. For the IH, the spectrum does not show the individual peaks, is narrower than the one for the CO, but is wider than the sphere that shows a single peak, which corresponds to the dipolar SPR.

In summary, it was found that as the truncation  $r$  increases (i) the main resonance is always blue-shifted, (ii) the SPRs at smaller wavelength are closer to the dominant mode, so they can be hidden, and (iii) the width of the main SPRs increases. For instance, the full width at the half-maximum (fwhm) of the TC with  $1/8$  is about 70 nm, whereas the one with  $r = 1/2$  (CO) is about 115 nm. This means that the secondary resonances do not disappear but are closer to the dominant SPR, producing wider spectra at larger truncations. For the IH and the sphere, the fwhm are about 60 and 20 nm, respectively. This indicates that the SPRs vanish as the number of faces increases or when the symmetry of the NP is greater. The resonance of the sphere is always at the smallest wavelength, whereas the main SPR of the IH is blue-shifted with respect of the cubes but at a larger wavelength of the sphere. Then, as the number of faces of the NP increases (i) there are fewer SPRs, (ii) the main resonance is blue-shifted, and (iii) the fwhm of the spectra decreases.

**B. Decahedral Morphology.** Another important morphology present in metal NPs is the DH or pentagonal bipyramid, which is obtained by different synthesis methods.<sup>21–26</sup> The regular DH,

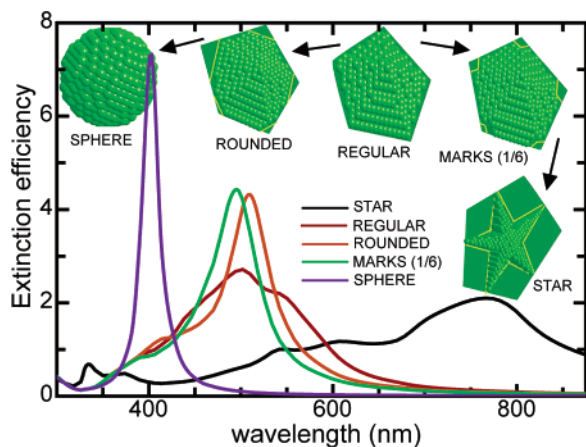


**Figure 6.** Extinction efficiency as a function of the wavelength of the incident light for the regular decahedron and its truncated morphologies for parallel light polarization.

shown in Figure 6, is composed of 10 planar triangular faces, which resemble two pentagons. However, when the NP's size is in the range between 1 and 5 nm, the regular DH is rarely observed, and the most common shapes are the truncated ones: the Marks and rounded DHs. The first structure was introduced by Marks<sup>81</sup> and is remarkably stable. In very clean growth conditions, or with weak interactions with substrates, this is one of the predominant shapes for the discussed size interval. A way to describe the Marks DH is as a regular DH, which has truncations on its facets, as shown in Figure 6. When the truncation reaches a maximum value, a morphology with the shape of a star DH is formed. Another type of DH NP, which is often observed, corresponds to the rounded pentagonal NP, in which the truncation has a minimum possible value producing a contrast reduction in the borders. This type of particle is frequently formed when colloidal growth methods are used.<sup>22</sup> Here, we briefly discuss the SPRs of the rounded dh with a truncation of  $r = 1/8$ , the Marks dh with  $r = 1/6$ , the star, and the regular DH. A more detailed discussion can be found in refs 27 and 80.

Due to the symmetry of the DH NP, two different polarizations of the incident electromagnetic field are present: when  $\vec{E}$  is parallel or perpendicular to the pentagonal motif. When the electric field is perpendicular to the pentagon of the regular DH, the spectrum shows a peak with its maximum at about 358 nm and has a fwhm of 90 nm. It was found that SPRs present at the perpendicular polarization are not affected with any truncation, except for the star DH,<sup>80</sup> where the main SPR is red-shifted by 100 nm and is 5.5 times more intense, and its fwhm is narrowed to 40 nm.<sup>80</sup> On the other hand, the parallel polarization is more sensitive to the different truncations. In Figure 6,  $Q_{\text{ext}}$  of the regular, rounded, Marks, and star DHs, when  $\vec{E}$  is parallel, are shown. The response of the star decahedral is totally different since it shows resonances in a very wide range of wavelengths. For the parallel polarization, the rounded decahedra show the same effect as a function of the truncation as observed in the case of truncated cubes. The main resonance is blue-shifted, and becomes the most intense peak after truncation.

## VI. Influence of Physical Environment on Surface Plasmons Resonances

We showed that with small changes of the morphology it is possible to tune the SPRs of NPs. Here, we want to study how these SPRs are influenced if the physical environment is modified. In this direction, we have already shown how the

SPRs are shifted if the dielectric properties of the surrounding media are changed. In particular, we showed that the SPRs in a medium with refractive index  $n > 1$  are red-shifted with respect to those in vacuum. Furthermore, this shift depends on the proper mode itself: the larger the wavelength of the eigenmode, the greater the red shift, and the more spread out the SPRs. However, we are interested not only in the case when the dielectric properties are changed but also when the physical environment of the NP becomes different. We wonder what happens to the SPRs when the particles lie on a substrate or when they are close enough that the dilute limit is no longer valid, and the electromagnetic interactions among NPs should be considered.

These two situations are of great importance in a large variety of problems that have promising technological applications, like surface-enhanced Raman scattering (SERS),<sup>82–84</sup> catalytic processes,<sup>85,86</sup> plasmonic devices,<sup>87,88</sup> and others. For instance, in the case of the electromagnetic effect in SERS, the anomalous enhancement of the optical response has been examined by adsorbing molecules at non-flat metallic surfaces and at NPs of different shapes. Although the optical spectra of adsorbed molecules might carry information about specific features of the molecular electronic structure or charge-transfer mechanisms, the information sought in the optical response of supported particles is related more to their shape, substrate-induced multipolar coupling, or local field effects. The calculation of the field at the surface of these NPs requires the full solution of the optical response problem.

In this section, we study two important systems where the physical environment of the isolated or suspended NPs is changed. First, we analyze the SPRs when the particle is placed above a substrate. Second, we examine the SPRs for a linear chain of NPs, which are close enough that they interact because of the local electromagnetic field.

**A. Supported Nanoparticles.** The optical response of metallic NPs deposited on a substrate is also characterized by the presence of SPRs. The location and broadening of these resonances depend on the geometrical and dielectric properties of the system. When the system is under the action of an external EM field, it induces a charge polarization on the particle that causes a charge distribution on the substrate, which in turn also affects the NP. In the quasistatic limit, this charge distribution can be seen as the image charge distribution of the NP, as shown in Figure 7. Although the dipolar approximation might be sufficient for describing the optical response of an isolated sphere, the substrate-induced field acting on the ample volume of the NP is no longer homogeneous in space, and multipolar modes of very high order might excite in addition to the dipole (see Figure 7b). The interaction between the NPs is also important, especially in the case of a high concentration of them. However, the study of a single supported particle can be also performed in the dilute regime.<sup>89–93</sup>

Different authors have included the multipolar interactions considering particles of different shapes;<sup>91–97</sup> however, the numerical complexity of the problem restricts the number of multipolar modes taken to describe the system. A powerful theoretical method was developed to calculate the optical response of a particle–substrate system using the spectral representation.<sup>91</sup> With this method, one is also able to include a larger number of multipoles, allowing the treatment of particles closer to the substrate. The inclusion of multipolar interactions between the particle and its image gives rise to resonances additional to the dipolar one. The structure of these resonances is more evident when the contrast between the dielectric

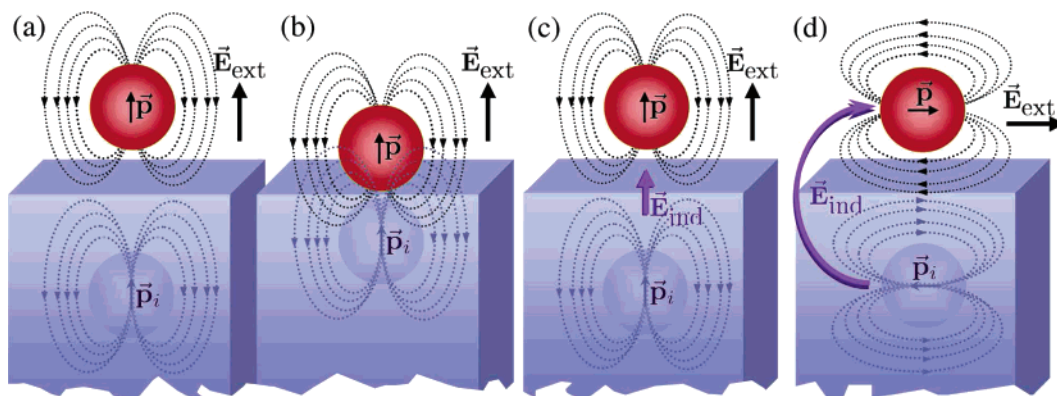


**Figure 7.** (a and b) Electromagnetic interaction between the NP and substrate as a function of the separation, modeled using the image method. Induced local field for an applied field (c) normal and (d) parallel to the interface.

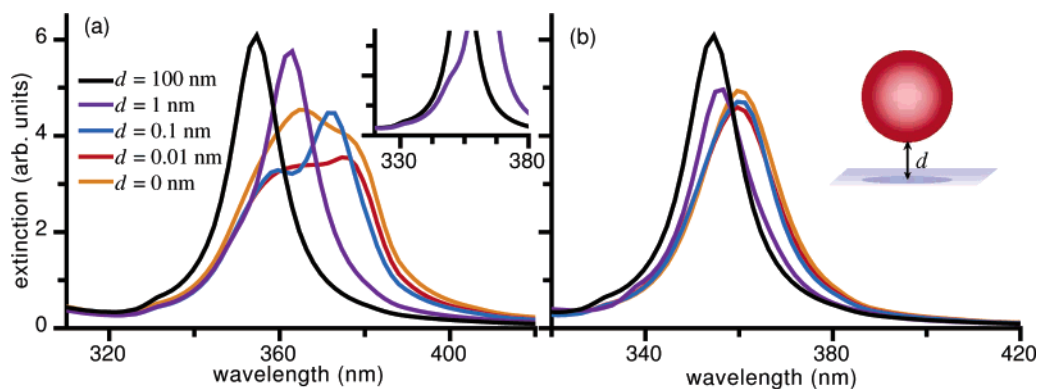


**Figure 8.** Extinction efficiency of silver spherical NPs located above the substrate by a distance  $d$ , for an external field (a) normal and (b) parallel to the substrate.

responses of the ambient and substrate increases.<sup>91</sup> For example, when a particle is in close contact with the substrate, smooth spectra are obtained. On the contrary, when the particle is located at a certain distance above the substrate, a well-defined structure of resonances is found.

Let us first analyze the optical response of a silver spherical NP of radius of 10 nm lying above a substrate of  $\text{Al}_2\text{O}_3$  with dielectric constant  $\epsilon_{\text{sub}} = 3.132$  and embedded in air. Due to the presence of the substrate, the symmetry of the system is broken and different proper modes can be found for light polarized parallel and normal to the interface. In Figure 8, we show  $Q_{\text{ext}}$  for light polarized (a) parallel and (b) normal to the substrate surface, where a spherical NP is located at different distances  $d$ . At  $d = 100$  nm, the interaction between NP and substrate is null, and the optical response corresponds to that of an isolated sphere, being the SPR the same for both polarizations. As the particle approaches the substrate, the multipolar excitations are evident since the spectra become wider and several peaks are observed. For instance, at  $d = 1$  nm and normal polarization, the dipolar SPR is red-shifted about 10 nm, and a secondary SPR at 346 nm with quadrupolar character is excited, giving rise to the shoulder shown in the inset. When the NP is touching the substrate,  $d = 0$  nm, we have taken 2000 multipolar interactions, where convergence has been partly reached.<sup>91</sup> For illustration purposes, we also show the case when  $d = 0.01$  nm that shows how sensitive the optical response of the normal modes is. When the particle is touching the substrate, the SPR with dipolar character shifts to larger wavelengths, and the coupling between multipolar modes become important; thus, more modes are excited and their individual character identity starts to disappear, such that, the spectra is twice as wide as the one of the isolated sphere, and the individual SPRs are not longer

observed. Note that as the radius of the sphere diminishes, the imaginary part of the NP dielectric function increases, such that, the broadening effects wash out the details of the resonant structure.<sup>92</sup> Thus, different spectra could be obtained considering particles of different material even if the geometry of the system is the same.<sup>93</sup>

Although the influence of the substrate is the same for both polarizations, the optical response to the applied field parallel to the substrate seems to be less sensitive to its presence. It has been found that the excited SPRs cover a more extended region of values when the applied field is normal to the surface than when it is parallel, and they are distributed more symmetrically in the first case.<sup>91</sup> Independently of the direction of the applied field, the spectra is always red-shifted as the particle approaches the substrate. This can be explained using the simple model depicted in Figure 7, panels c and d. When the external field is applied normal to the interface, shown in Figure 7c, it polarizes both particle and substrate in the same direction, such that, the induced local field acting on the particle is along the applied field and against the restoring forces, thus decreasing the frequency of the SPRs. When the field is applied parallel to the interface, Figure 7d, it polarizes the particle in the opposite direction to the substrate polarization, but the induced local field acting on the particle is also along the applied field and against the restoring forces, again decreasing the frequency of the SPRs.

Now, let us consider spheroidal NPs with their symmetry axis normal to the interface, located at a minimum distance  $d$ , and immersed in air. The same type of behavior of the mode spectra was found as for the case of the sphere, as the distance from the substrate is varied. Let us study the case when the NP is at a fixed distance, but its aspect ratio  $a/b$  varies. In Figure 9, we show  $Q_{\text{ext}}$  of a silver prolate at  $d = 0.01$  nm from a  $\text{TiO}_2$

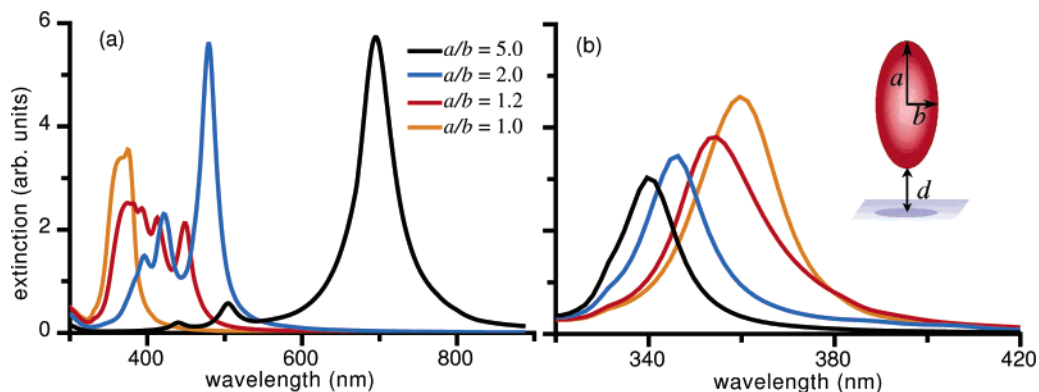


**Figure 9.** Extinction efficiency of silver prolates located at a distance  $d = 0.01$  nm, and different aspect ratios  $a/b$ , for an external field (a) normal and (b) parallel to the substrate.

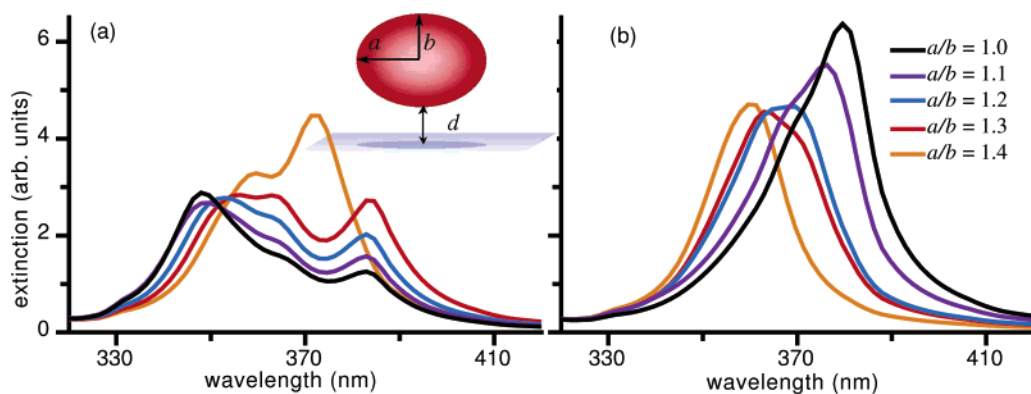


**Figure 10.** Extinction efficiency of silver oblates located at a distance  $d = 0.1$  nm, and different aspect ratios  $a/b$ , for an external field (a) normal and (b) parallel to the substrate.

substrate with dielectric constant  $\epsilon_{\text{sub}} = 7.8$ . In this particular geometry, the normal polarization excites the longitudinal modes (LMs), whereas the parallel polarization excites the transversal modes (TMs) of prolates, as defined in section IV. We observe that the LMs are red-shifted as the aspect ratio  $a/b$  increases, whereas the TMs are blue-shifted, corroborating our previous findings for the suspended prolates. One can see that, as the ratio  $a/b$  increases, a dominant mode appears, which turns out to lie very close to the dipolar mode of the suspended spheroid. This means that as  $a/b$  increases the spheroid actually decouples from the substrate. In contrast, as  $a/b \rightarrow 1$ , the dominant mode merges down and the mode-strength distribution becomes broader and equal to that found for the sphere. In conclusion, we observe that multipolar effects become more important as  $a/b$  tends to unity, that is, when the actual shape tends to be spherical.

The dependence of the spectra with the distance between particle and substrate is similar for oblate spheroids as for spheres and prolates. This means that the multipolar effects due to the substrate acting on the particle are more important when particle and substrate are in contact, and their importance decreases as the particle recedes from the substrate. In Figure 10, we show  $Q_{\text{ext}}$  of silver oblates at a fixed distance  $d = 0.1$  nm from a substrate with dielectric constant  $\epsilon_{\text{sub}} = 4.7$ . Now, the normal polarization excites the transversal modes (TMs), whereas the parallel polarization excites the longitudinal modes (LMs). One can see that as  $a/b$  increases the spectra centroid for the normal (parallel) field shifts toward larger (smaller) wavelengths, and as the eccentricity increases, a tendency toward the appearance of a dominant mode is stronger for the field parallel to the substrate than for the normal one.

In conclusion, it was found that the multipolar effects on the optical properties of a NP due to the presence of a substrate depend on the direction of the applied external field. We have found that, for oblate and prolate particles with aspect ratio  $a/b > 3$ , the multipolar effects are reduced and the dipolar approximation gives a good description of the behavior of the system. Since multipolar effects become more important for systems where the substrate has a large dielectric constant, in this case, the dipolar approximation is not good enough. We have also shown that very different spectra could be obtained considering particles of different material even if the geometry of the system (i.e., the semi-axes and the distance) is the same. Finally, it was also found that the interpretation of the optical spectra could be helpful to elucidate the shape, size and distance of the NPs. Recent experiments in supported silver NPs have reproduced our results discussed in this section.<sup>97–100</sup>

**B. One-Dimensional (1D) Nanostructures.** There is intense and growing interest in one-dimensional (1D) nanostructures from the perspective of their synthesis and unique properties, especially with respect to their excellent optical response. Controlled patterning and alignment of nanostructures is critical for studying fundamental collective properties and for incorporating these promising materials into nanoelectronic, sensing, optoelectronic, and plasmonic devices. Several methods have been employed to align 1D structures, either from solutions/suspensions of the materials postsynthesis, in substrates, as well as using more sophisticated methods as ion beam implantation in solid matrices. In these systems, one crucial question is how important is the interaction among particles.

Here, the effective dielectric response for a 1D chain of interacting identical NPs is studied. We do this within the

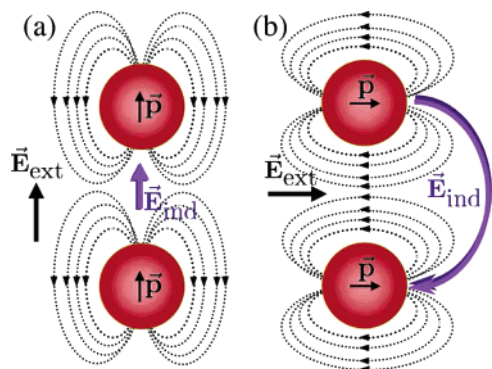


**Figure 11.** Model of the induced local field for an applied field (a) parallel and (b) transversal to the NPs chain.

quasistatic limit, and we perform a systematic study for different types of disorder and for filling fractions covering the whole range, from the extreme-dilute to the closed-packed limits. Our objective is twofold, (i) we want to study the properties of an 1D system due to the intrinsic interest that exists in the behavior of low-dimensional systems and (ii) we want to shed some light into the possible dependence of the effective dielectric response on the type of disorder. This allows us to analyze fluctuations induced in the local field by the positional disorder of the NPs. We employed the spectral representation to calculate the modes, and the details can be found elsewhere.<sup>102,103</sup>

When spherical NPs are aligned along a particular direction, the symmetry of the system is broken, and different proper modes can be found for light polarized parallel and perpendicular to the chain. When the external field is parallel, it polarizes the particles, such that, the induced local field is in the same direction as the applied field, see Figure 11a, and against the restoring forces, thus decreasing the frequency of the SPRs. When the field is perpendicular to the chain, shown in Figure 11b, it polarizes the induced local field against the applied field, but in the same direction of the restoring forces, thus increasing the frequency of the SPRs.

To understand the influence of the physical environment, results are presented for the extinction efficiency  $Q_{\text{ext}}$  as a function of wavelength, for the ordered case and two different

kinds of disorder (A and B), and for different filling fractions. In disorder A, we randomly move the NPs within an interval  $2\delta$  from the positions of a periodic chain. The parameter  $0 \leq \delta \leq 1/2$  serves as a measure of the disorder, for example,  $\delta = 0$  corresponds to the ordered case and  $\delta = 1/2$  to the maximum allowed disorder of this type. The disorder type B corresponds to random positions with the only restriction that NPs do not overlap. The choice of these types of disorder has nothing in particular; the idea is simply to illustrate the sensitivity of the optical response to a specific type of disorder algorithm, although some similar behaviors can be found. For example, (i) when a periodic 1D crystal is heated up, such that, the atoms move randomly around their ordered positions, or (ii) when the system is heated up and suddenly cooled down, such that, random positions without any correlation can be found.

In Figure 12, the influence of disorder is shown at different filling fractions. The nanospheres of 20 nm of radii are made of silver and embedded in air, and we have set  $\delta = 1/2$  for disorder A. We consider an external field parallel to the chain. The case when the external field lies transversal to the chain will not be reported in this work; nevertheless, our study showed that in this case the corresponding disorder and multipolar effects are similar but less pronounced. In Figure 12a, the extinction for an ordered NP chain for three different filling fractions is shown. In the ordered case and dilute limit ( $f \rightarrow 0$ ), the proper modes of the system become equal to the multipolar resonances of the isolated sphere, where for small and medium filling fractions the dipolar mode is dominant. For a finite  $f$ , the eigenmodes are shifted due to the coupling of the spheres through fields of the same multipolar order. Upon interaction, the individual multipolar character is lost. One should notice that, due to the symmetry of the ordered chain, the interacting fields of multipoles of even order are canceled. Therefore, at  $f = 0.8$  also the octupolar fields are important. As  $f$  increases, the proper modes have a monotonic red (blue) shift when the field is parallel (transversal) to the chain. In Figure 12, we appreciate that the larger the disorder, the larger the shift, and the multipolar fluctuations, instead of few resonances, excite a continuum distribution of them. This makes the multipolar coupling more efficient. In Figure 12b for disorder A more

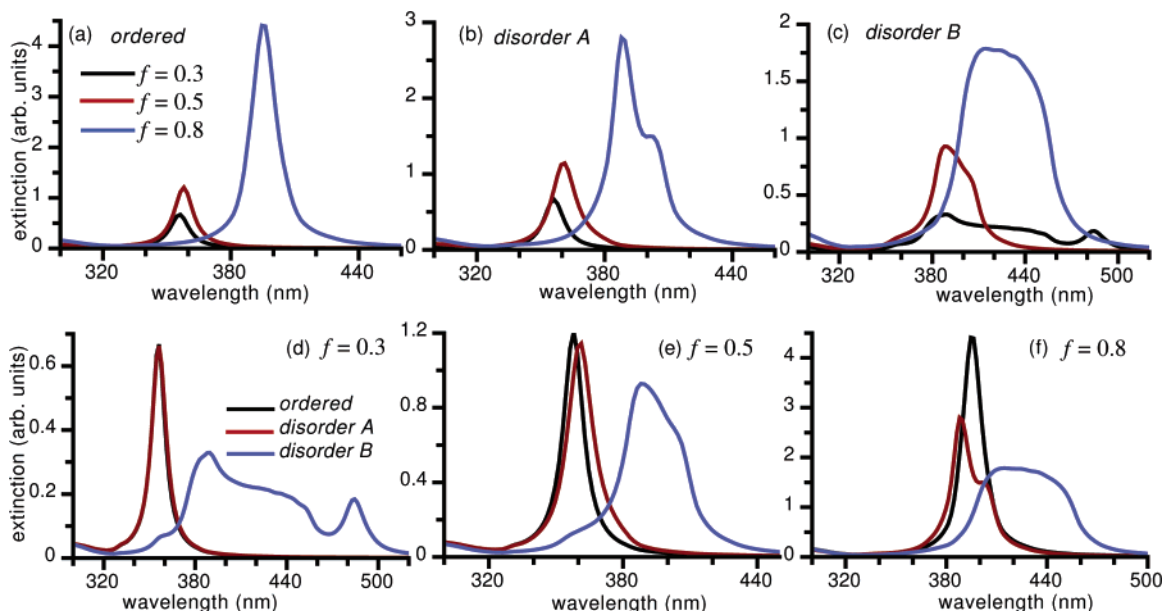


**Figure 12.** Extinction efficiency of a 1D chain of metal NPs at different filling fractions, for an external field parallel to the chain axis. The upper panels a–c correspond to the ordered chain and disorders A and B, respectively. The lower panels d–f corresponds to filling fractions  $f = 0.3, 0.5,$  and  $0.8,$  respectively.

resonances are observed only at  $f = 0.8$ , whereas for disorder B, shown in Figure 12c, the multipolar character is evident at any filling fraction. Notice that for larger filling fractions and greater disorder the dipolar character of the resonant mode is lost.

In conclusion, we found that as the filling fraction increases, more multipolar interactions are present, for all the positional arrangements. As the positional disorder increases, it also induces the excitation of new multipolar contributions. It seems that the spectrum becomes wider as there is more "room" for disorder. As a consequence, the inclusion of these multipolar modes shifts the main peak to higher (lower) wavelengths and increases the extension of the tail in the low (high)-wavelength side, for an external field parallel (transversal) to the chain. But the most interesting thing is that there is not only a red shift of the peaks but also a drastic change in the profile. Furthermore, it was found that, due to the symmetry of the system, there is no coupling between the directions parallel and transversal to the chain. This means that an external field parallel to the chain will induce multipoles in each sphere, with an axis of symmetry also parallel to the chain, but they will fluctuate in magnitude and phase. These fluctuations cause the existence of a manifold of collective modes with a continue range of resonant frequencies.

## VII. Summary and Future Trends

We have studied the general behavior of the surface plasmon resonances on small metal NPs in terms of their shape and physical environment. For instance, the location of these resonances on NPs of different shapes has been studied and has been found that NPs with fewer faces and sharper vertices show resonances in a wider range of wavelengths. We also showed that, when a NP is truncated, the main resonance is blue-shifted, overlapping secondary resonances and, therefore, increasing the full width at half-maximum. However, for decahedral particles, the truncation to Marks and rounded decahedra shows the same blue shift effect, but the full width at half-maximum decreases, perhaps because the secondary resonances no longer exist as the number of faces increases. We also explained in detail the optical anisotropy of elongated NPs, such as, ellipsoids, decahedra, etc., where the dependence of the position of the resonances is analytically explained in terms of their aspect ratio.

We have analyzed the case where noninteracting elongated NPs are aligned in a given direction, such that, the optical response can be tuned using polarized light and changing the aspect ratio. We also studied the case of a linear chain of interacting NPs, where again, the surface plasmon resonances are sensitive to the light polarization, and their dependence with the positional disorder of the particles. This 1D nanostructures can be the starting point for more complex structures. Finally, the case of supported NPs was also studied. In this case, the line-shape of the spectra, and its relation with high-multipolar excitation, is studied in detailed for ellipsoidal NPs. The optical response is studied for different physical situations: as a function of the distance between the particle and substrate, as well as in terms of the anisotropy of the particle.

This information would be useful to motivate the development of more complex nanostructures with tunable surface plasmon resonances. For this, it would be desirable to develop a simple theory capable of predicting the position and strength of the SPRs of an ample variety of NPs shapes and physical environments. We have already mentioned that the spectral representation formalism completes with these characteristics, because it

separates the contribution of the dielectric properties from the geometrical ones. We have shown the potentiality of this theory, that allows us to perform a systematic study of the optical response of NPs, once a shape is chosen. However, explicit expressions of the spectral representation are difficult to obtain, but alternative forms could be found.

**Acknowledgment.** I am in debt to my many colleagues and students that have contributed along these years to the study of the optical response on nanoparticles. In particular, I would like to acknowledge Professor Rubén G. Barrera and Dr. Carlos E. Román for their illuminating contributions in spectral representation formalism and substrate effects. I also want to acknowledge the contribution of Ana Lilia González in the study of the polyhedral particles. Partial financial support from CONACyT Grant Nos. 48521-F and 44306-F and DGAPA-UNAM Grant No. IN101605 is also acknowledged.

## References and Notes

- (1) Noguez, C.; Román-Velázquez, C. E. *Phys. Rev. B* **2004**, *70*, 195412.
- (2) Intravaia, F.; Lambrecht, A. *Phys. Rev. Lett.* **2005**, *94*, 110404.
- (3) Xu, H.; Käll, M. *Phys. Rev. Lett.* **2002**, *89*, 2468021.
- (4) Ozbay, E. *Science* **2006**, *331*, 189.
- (5) Maier, S. A.; Kik, P. G.; Atwater, H. A.; Meltzer, S.; Harel, E.; Koel, B. E.; Requicha, A. A. G. *Nat. Mat.* **2003**, *2*, 229.
- (6) Maier, S. A.; Atwater, H. A. *J. Appl. Phys.* **2005**, *98*, 011101.
- (7) Zhang, Y.; Gu, C.; Schwartzberg, A.; Chen, S.; Zhang, J. Z. *Phys. Rev. B* **2006**, *73*, 1654051.
- (8) Haynes, C. L.; McFarland, A. D.; Van Duyne, R. P. *Anal. Chem.* **2005**, *77*, 338A.
- (9) Jin, R.; Cao, Y.; Mirkin, C. A.; Kelly, K. L.; Schatz, G. C.; Zheng, J.-G. *Science* **2001**, *294*, 1901.
- (10) Jin, R.; Cao, Y. C.; Hao, E.; Métraux, G. S.; Schatz, G. C.; Mirkin, C. A. *Nature* **2003**, *425*, 487.
- (11) Sönnichsen, C.; Reinhard, B. M.; Liphardt, J.; Alivisatos, A. P. *Nat. Biotechnol.* **2005**, *33*, 741.
- (12) Hibbins, A. P.; Evans, B. R.; Sambles, J. R. *Science* **2005**, *308*, 670.
- (13) Liz-Marzán, L. M. *Langmuir* **2006**, *22*, 32.
- (14) Barnes, W. L.; Dereux, A.; Ebbesen, T. W. *Nature* **2003**, *424*, 824.
- (15) Huang, X.; El-Sayed, I. H.; Qian, W.; El-Sayed, M. A. *J. Am. Chem. Soc.* **2006**, *128*, 2115.
- (16) Kelly, K. L.; Coronado, E.; Zhao, L. L.; Schatz, G. C. *J. Phys. Chem. B* **2003**, *107*, 668.
- (17) Sosa, I. O.; Noguez, C.; Barrera, R. G. *J. Phys. Chem. B* **2003**, *107*, 6269.
- (18) Noguez, C. *Opt. Mat.* **2005**, *27*, 1204.
- (19) Payne, E. K.; Shuford, K. L.; Park, S.; Schatz, G. C.; Mirkin, C. A. *J. Phys. Chem. B* **2006**, *110*, 2150.
- (20) Lee, K.-S.; El-Sayed, M. A. *J. Phys. Chem. B* **2005**, *109*, 20331.
- (21) Wang, Z. L. *J. Phys. Chem. B* **2000**, *104*, 1153.
- (22) Yacamán, M. J.; Ascencio, J. A.; Liu, H. B.; Gardea-Torresdey, J. *J. Vac. Sci. Technol. B* **2001**, *19*, 1091.
- (23) Yang, C. Y. *J. Cryst. Growth* **1979**, *47*, 274.
- (24) Kuo, C.-H.; Chiang, T.-F.; Chen, L.-J.; Huang, M. H. *Langmuir* **2004**, *20*, 7820.
- (25) Wei, G.; Zhou, H.; Liu, Z.; Song, Y.; Wang, L.; Sun, L.; Li, Z. *J. Phys. Chem. B* **2005**, *109*, 8738.
- (26) Nilius, N.; Ernst, N.; Freund, H.-J. *Phys. Rev. Lett.* **2000**, *84*, 3994.
- (27) Gonzalez, A. L.; Noguez, C.; Ortiz, G. P.; Rodriguez-Gattorno, G. *J. Phys. Chem. B* **2005**, *109*, 17512.
- (28) Tao, A.; Sinsersuksakul, P.; Yang, P. *Angew. Chem., Int. Ed.* **2006**, *45*, 4597.
- (29) Baletto, F.; Ferrando, R. *Rev. Mod. Phys.* **2005**, *77*, 371.
- (30) Barnard, A. S.; Lin, X. M.; Curtiss, L. A. *J. Phys. Chem. B* **2005**, *109*, 24465.
- (31) Román-Velázquez, C. E.; Noguez, C.; Garzón, I. L. *J. Phys. Chem. B* **2003**, *107*, 12035.
- (32) Sánchez-Castillo, A.; Román, Velázquez, C. E.; Noguez, C. *Phys. Rev. B* **2006**, *73*, 045401.
- (33) Yao, H.; Miki, K.; Nishida, N.; Sasaki, A.; Kimura, K. *J. Am. Chem. Soc.* **2005**, *127*, 15536.
- (34) Negishi, Y.; Nobusada, K.; Tsukuda, T. *J. Am. Chem. Soc.* **2005**, *127*, 5261.
- (35) Nobusada, K. *J. Phys. Chem. B* **2004**, *108*, 11904.

- (36) Negishi, Y.; Takasugi, Y.; Sato, S.; Yao, H.; Kimura, K.; Tsukuda, T. *J. Am. Chem. Soc.* **2004**, *126*, 6518.
- (37) Fuchs, R. *Phys. Rev. B* **1975**, *11*, 1732.
- (38) Bergman, D. *Phys. Rep.* **1978**, *43*, 377.
- (39) Milton, G. W. *Appl. Phys. Lett.* **1980**, *37*, 300.
- (40) Barrera, R. G.; Noguez, C.; Anda, E. V. *J. Chem. Phys.* **1992**, *96*, 1574.
- (41) Bohren, C. F.; Human, D. R. *Absorption and Scattering of Light by Small Particles*; John Wiley & Sons: New York, 1983.
- (42) Mie, G. *Ann. Phys.* **1908**, *25*, 377.
- (43) Kreibig, U.; Vollmer, M. *Optical properties of metal clusters*; Springer-Verlag: Berlin, 1995.
- (44) Asano, S.; Yamamoto, G. *Appl. Opt.* **1980**, *14*, 29.
- (45) Lind, A. C.; Greenberg, J. M. *J. Appl. Phys.* **1966**, *37*, 3195.
- (46) Mishchenko, M. I.; Hovenier, J. W.; Travis, L. D. *Light Scattering by Nonspherical Particles*; Academic Press: San Diego, 2000.
- (47) Gans, R. *Ann. Physik* **1912**, *37*, 881; **1915**, *47*, 270.
- (48) Van de Hulst, H. C. *Light Scattering by Small Particles*; John Wiley & Sons: New York, 1957.
- (49) Johnson, P. B.; Christy, R. W. *Phys. Rev. B* **1972**, *6*, 4370.
- (50) Coronado, E. A.; Schatz, G. C. *J. Chem. Phys.* **2003**, *119*, 3926.
- (51) Kreibig, U. *J. Phys. F: Met. Phys.* **1974**, *4*, 999.
- (52) Purcell, E. M.; Pennypacker, C. R. *Astrophys. J.* **1973**, *186*, 705.
- (53) Draine, B. T. *Astrophys. J.* **1988**, *333*, 848.
- (54) Draine, B. T.; Goodman, J. *Astrophys. J.* **1993**, *405*, 685.
- (55) Draine, B. T.; Flatau, P. J. *J. Opt. Am. A* **1994**, *11*, 1491.
- (56) Draine, B. T.; Flatau, P. T. *Source code DDSCAT 6.0*, <http://www.astro.princeton.edu/~draine/DDSCAT.html>.
- (57) Kumbhar, A. S.; Kinnan, M. K.; Chumanov, G. *J. Am. Chem. Soc.* **2005**, *127*, 12444.
- (58) Meier, M.; Wokaun, A. *Opt. Lett.* **1983**, *8*, 581.
- (59) Al-Sayed, A.-M.; Majied, A.-S. *Colloids Surf. A* **2004**, *246*, 61.
- (60) Lee, K.-S.; Al-Sayed, A.-M. *J. Phys. Chem. B* **2005**, *109*, 20331.
- (61) Perez-Juste, J.; Liz-Marzan, L. M.; Carnie, S.; Chan, D. Y. C.; Mulvaney, P. *Adv. Funct. Mater.* **2004**, *14*, 571.
- (62) Gou, L.; Murphy, C. J. *Chem. Mater.* **2005**, *17*, 3668.
- (63) Murphy, C. J.; Jana, N. R. *Adv. Mater.* **2002**, *14*, 80.
- (64) Brioude, A.; Jiang, X. C.; Pileni, M. P. *J. Phys. Chem. B* **2005**, *109*, 13138.
- (65) Jiang, X. C.; Brioude, A.; Pileni, M. P. *Colloids Surf. A* **2006**, *277*, 201.
- (66) Brioude, A.; Pileni, M. P. *J. Phys. Chem. B* **2005**, *109*, 23371.
- (67) Xu, X.; Cortie, M. B. *Adv. Funct. Mater.* **2006**, *6*, 2170.
- (68) Orendorff, C. J.; Murphy, C. J. *J. Phys. Chem. B* **2006**, *110*, 3990.
- (69) Penninkhof, J. J.; van Dillen, T.; Roorda, S.; Graf, C.; van Blaaderen, A.; Vredenberg, A. M.; Polman, A. *Nucl. Instrum. Methods B* **2006**, *242*, 523.
- (70) Oliver, A.; Reyes-Esqueda, J. A.; Cheang-Wong, J. C.; Román-Velázquez, C. E.; Crespo-Sosa, A.; Rodríguez-Fernández, L.; Seman, J. A.; Noguez, C. *Phys. Rev. B* **2006**, *74*, 245425.
- (71) Cortie, M. B.; Xu, X.; Ford, M. J. *Phys. Chem. Chem. Phys.* **2006**, *8*, 3520.
- (72) Murphy, C. J.; Sau, T. K.; Gole, A. M.; Orendorff, C. J.; Gao, J.; Gou, L.; Hunyadi, S. E.; Li, T. *J. Phys. Chem. B* **2005**, *109*, 13857.
- (73) Pérez-Juste, J.; Pastoriza-Santos, I.; Liz-Marzan, L. M.; Mulvaney, P. *Coord. Chem. Rev.* **2005**, *249*, 1870.
- (74) Lifshitz, E. M.; Landau, L. D.; Pitaevskii, L. P. *Electrodynamics of Continuous Media*, 2nd ed.; Butterworth-Heinemann: Burlington, MA, 1984.
- (75) Sun, Y.; Xia, Y. *Science* **2002**, *298*, 2176.
- (76) Zhou, M.; Chen, S.; Zhao, S. *J. Phys. Chem. B* **2006**, *110*, 4510.
- (77) Chen, Y.; Gu, X.; Nie, C.-G.; Jiang, Z.-Y.; Xie, Z.-X.; Lin, C.-J. *Chem. Comm.* **2006**, *33*, 4181.
- (78) Salzemann, C.; Brioude, A.; Pileni, M.-P. *J. Phys. Chem. B* **2006**, *110*, 7208.
- (79) Banerjee, I. A.; Yu, L.; Matsui, H. *Proc. Natl. Acad. Sci.* **2003**, *100*, 14678.
- (80) González, A. L.; Noguez, C. *J. Comp. Theor. Nanosci.* **2007**, *4*, 273.
- (81) Marks, L. D. *Rep. Prog. Phys.* **1994**, *57*, 603.
- (82) Haes, A. J.; Haynes, C. L.; McFarland, A. D.; Zou, S.; Schatz, G. C.; Van Duyne, R. P. *MRS Bull.* **2005**, *30*, 368.
- (83) Schatz, G. C.; Young, M. A.; Van Duyne, R. P. *Surface Enhanced Raman Scattering Physics and Applications*. In *Topics in Applied Physics*; Kneipp, K., Moskovits, M., Kneipp, H., Eds.; Springer: New York, 2006; Vol. 103, pp 19–46.
- (84) Dieringer, J. A.; Lyandres, O.; McFarland, A. D.; Shah, N. C.; Stuart, D. A.; Whitney, A. V.; Yonzon, C. R.; Young, M. A.; Yuen, J.; Zhang, X.; Van Duyne, R. P. *Faraday Discuss.* **2006**, *132*, 9.
- (85) Haruta, M.; Kageyama, H.; Kamijo, N.; Kobayashi, T.; Delannay, F. *Stud. Surf. Sci. Catal.* **1988**, *44*, 33.
- (86) Haruta, M.; Kobayashi, T.; Sano, H.; Yamada, N. *Chem. Lett.* **1987**, *2*, 405.
- (87) Li, K.; Stockman, M. I.; Bergman, D. J. *Phys. Rev. Lett.* **2005**, *72*, 153401.
- (88) Cvitkovic, A.; Ocelic, N.; Aizpurua, J.; Guckenberger, R.; Hillenbrand, R. *Phys. Rev. Lett.* **2006**, *97*, 060801.
- (89) Beitia, C.; Borensztein, Y.; Lazzari, R.; Nieto, J.; Barrera, R. G. *Phys. Rev. B* **1999**, *60*, 6018.
- (90) Beitia, C.; Borensztein, Y.; Barrera, R. G.; Román, C. E.; Noguez, C. *Physica B* **2000**, *279*, 25.
- (91) Román-Velázquez, C. E.; Noguez, C.; Barrera, R. G. *Phys. Rev. B* **2000**, *61*, 10427.
- (92) Román-Velázquez, C. E.; Noguez, C.; Barrera, R. G. *Phys. Status Solidi (a)* **1999**, *175*, 393.
- (93) Román, C. E.; Noguez, C.; Barrera, R. G. *MRS Symp. Proc.* **2000**, *581*, 485.
- (94) Wind, M. M.; Vlieger, J.; Bedeaux, D. *Physica A* **1987**, *141*, 33.
- Wind, M. M.; Bobbert, P. A.; Vlieger, J.; Bedeaux, D. *Physica A* **1987**, *143*, 164.
- (95) Ruppin, R. *Phys. Rev. B* **1992**, *45*, 11209.
- (96) Bobbert, P. A.; Vlieger, J. *Physica A* **1986**, *137*, 243.
- (97) Bedeaux, D.; Vlieger, J. *Optical properties of surfaces*; Imperial College Press: London, 2004.
- (98) Lazzari, R.; Roux, S.; Simonsen, I.; Jupille, J.; Bedeaux, D.; Vlieger, J. *Phys. Rev. B* **2002**, *65*, 235424.
- (99) Lazzari, R.; Simonsen, I.; Jupille, J. *Europhys. Lett.* **2003**, *61*, 541.
- (100) Lazzari, R.; Jupille, J.; Layet, J. M. *Phys. Rev. B* **2003**, *68*, 045428.
- (101) Xu, G.; Tazawa, M.; Jin, P.; Nakao, S. *Appl. Phys. A* **2005**, *80*, 1535.
- (102) Noguez, C.; Barrera, R. G. *Phys. Rev. B* **1998**, *57*, 302.
- (103) Noguez, C.; Barrera, R. G. *Physica A* **1994**, *211*, 399.